A Distributed Feedforward Control Method for Power Electronic Transformers

Sizhao Lu, *Member, IEEE*, Di Zhao, Kai Li, *Member, IEEE*, and Siqi Li, *Member, IEEE*

***Abstract*—Because of its advantages such as small size and light weight, power electronic transformers (PET) are increasingly used in power transmission and distribution systems. The traditional centralized control method requires each cascaded power module to communicate with the central controller through a high-speed communication link, which increases the computational and communication burden of the central controller and reduces the expandability and modularity of a PET system. In this paper, a distributed feedforward control method for a cascaded H-bridge (CHB) converter-based PET is proposed. The pulse width modulation, input current regulation, voltage balance control, power balance control, output voltage regulation and output current regulation are assigned to the distributed local controllers. Therefore, the computational and communication burden of the central controller can be significantly reduced. The number of fibers connected to the central controller can be significantly reduced. Meanwhile, the proposed control method can greatly improve the dynamic response of the load disturbance, and a smooth start-up process of the PET system can be achieved. Simulation results are given to show the effectiveness of the proposed method.**

***Index Terms*—Cascaded H-bridge (CHB) converter; power electronic transformers (PET); distributed feedforward control.**

I. INTRODUCTION

POWER electronic transformer (PET) is a new type of electrical equipment that can realize harmonic elimination, voltage compensation, device self-protection, and power conversion between different AC and DC voltage levels [1]-[4]. The cascaded H-bridge (CHB) converter has the characteristics of high modularity, scalability and easy redundancy design [1], which makes it become a popular circuit topology in PET system.

For PET, a centralized or distributed control system can be adopted to achieve the control goal [5], [6]. The centralized control method can accurately monitor the operating status of the systems and it is easier to realize system control and synchronized modulation [7], [8]. However, the centralized control requires each cascaded power module to communicate with the central controller through a high-speed communication link, which increases the computational and communication burden of the central controller, reduces the modularity and scalability of a PET system [9]. Therefore, the distributed control is more suitable for the PET system with a large number of cascaded power modules.

The distributed control can be realized as central-local distributed architecture [6] or master-slave distributed architecture [10]. For the central-local distributed architecture, a central controller and many local controllers are employed, the system-level control and internal dynamics control tasks are assigned to either the central controller or the local controller. In [6], a central controller is employed only to realize the system-level output power control and protection for a modular multilevel converter (MMC), the local controllers process the tasks such as submodule capacitor voltage balance, differential current regulation, PWM generation and local protection. Therefore, the communication burden of the communication network is significantly reduced because the data interaction among the central controller and the local controllers is greatly reduced. For the cascaded STACOM, the central controller can even be eliminated, and the individual local controller makes the decisions to control each cascaded power module [11]. The reactive power sharing, DC-link voltage balancing and autonomous frequency synchronization can be achieved. However, an input AC capacitor is needed for each power module and the system-level protection is not investigated in this paper. In [12], a decentralized control strategy for a modular cascaded converter is proposed, where the switching actions and the current regulation are realized by the local controller based on the local sensors and the local modulator. The master controller only takes charge of coordination, reference generation and global protection. For the master-slave distributed architecture, one of the power module controller is adopted as the master controller, which processes the tasks of the system-level control with only one power module's information and distributes the common duty cycle to all other slave controllers. The slave controller also controls the isolation DC-DC converter in each cascaded power module [10]. A hierarchical distributed control architecture for the CHB converters is proposed in [9]. Current tracking is performed through the master control, and the slave control based on consensus algorithm is adopted in order to achieve power balance among modules. In the previous literatures, the

Manuscript received September 05, 2020; Revised November 15, 2020; Accepted December 15, 2020. Date of publication December 25, 2020; Date of current version December 18, 2020.

This work was supported in part by the National Natural Science Foundation of China under Grant 51707088." (*Corresponding Author: Siqi Li*)

Sizhao Lu, Di Zhao and Siqi Li are with the Department of Electrical Engineering, Kunming University of Science and Technology, Kunming, 650500, China. (e-mail: lusz10@ kust.edu.cn).

Kai Li is with the Department of Electrical Engineering, Beijing Jiaotong University, Beijing, 100044, China. (e-mail: kaili@bjtu.edu.cn).

Digital Object Identifier 10.30941/CESTEMS.2020.00039

2096-3564 © 2020 CES

distributed control is mainly implemented in the single-stage converter, such as CHB converters and MMCs. Meanwhile, few of papers focus on the dynamic response of the CHB converter-based PET with the distributed control. The main contributions of this paper are as follows:

1) A novel distributed feedforward control method is proposed for CHB converter-based PET, which can balance the voltage and power of each module. Meanwhile, the distributed control mode can effectively reduce the number of fibers connected to the central controller. In addition, the proposed control method can significantly reduce the calculation and communication burden of the central controller, and improve the system scalability and expandability.

2) Feedforward control is added to the distributed control method which can effectively improve the dynamic response of the system. The PET system can quickly achieve its steady-state after the load disturbance and a smooth start-up process of the PET system is also achieved.

This paper is organized as follows: Section II introduces the CHB converter based the PET topology. Section III proposes a distributed feedforward control strategy, which is applied to CHB converter-based PET. Simulation results are given in Section IV and the conclusion is drawn in section V.

II. Main Circuit of CHB Converter Based PET

The main circuit of the CHB converter-based PET is shown in Fig. 1, which is composed of three phases. Each phase is composed of a CHB and an input-series-output-parallel connected dual active bridge (DAB) converter. The output of the DAB converter is followed by a three-phase inverter. The CHB converter in the rectifier stage is built by low voltage rating power devices and it can be directly connected to the medium voltage (MV) grid. The output voltage of the CHB is a multilevel stair case waveform, so a good power quality of the MV grid side can be achieved. High frequency transformers are employed in the DAB converters, which transfer the power and provide the galvanic isolation between the high DC voltage side to the low-voltage DC bus. The rated voltage and rated power of the system can be expanded by using more cascaded power modules [13]. Meanwhile, the low-voltage DC bus and the low-voltage AC port can be connected to different electrical facilities with bidirectional power flow. [14]. The low-voltage DC bus can be connected to renewable energy sources or DC loads. The low voltage port can be connected to the low voltage AC grid or AC loads.

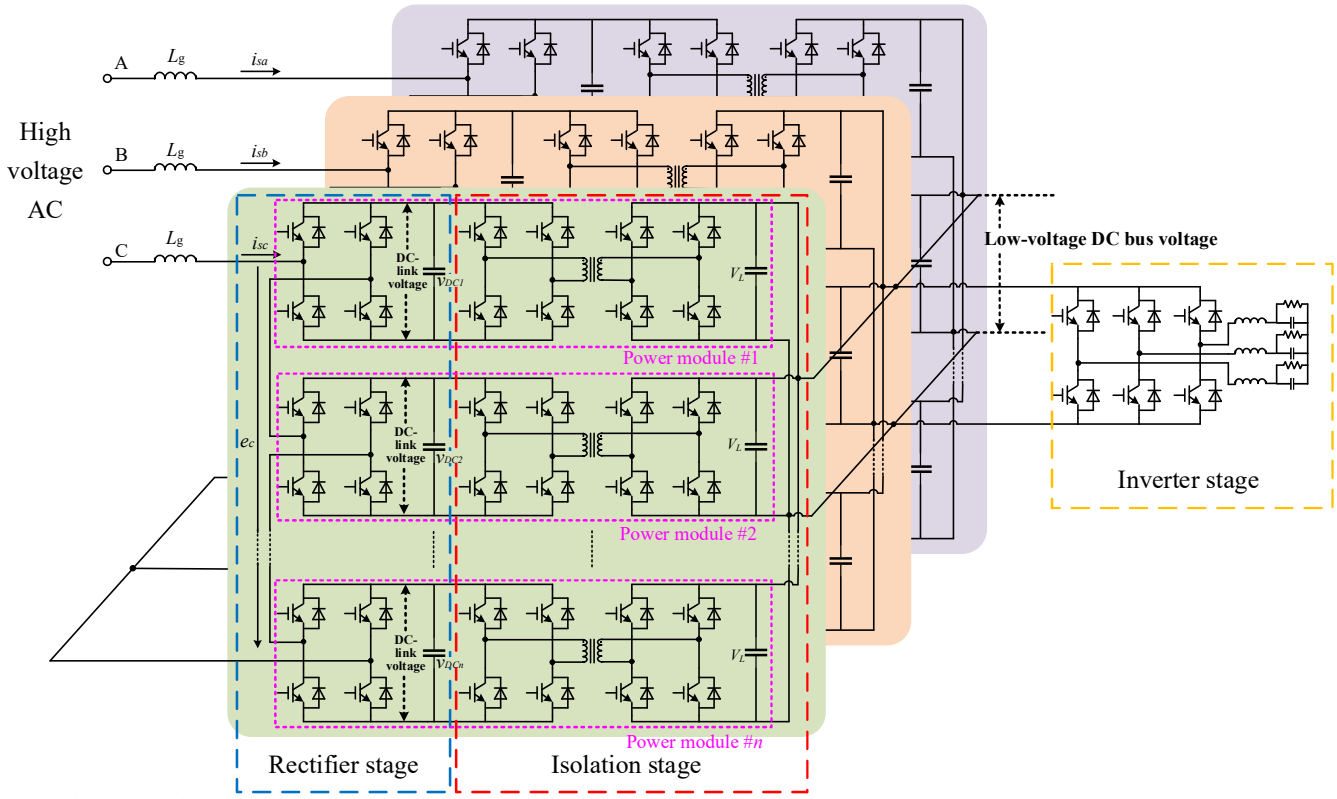

Fig. 1. Topology of PET based on CHB.

III. Distributed Feedforward Control Strategy of CHB Converter-Based PET

The structure of the proposed distributed feedforward control for CHB converter-based PET is illustrated in Fig. 2. In Fig. 2, $V_{H\text{-}ref}$ is the reference of the DC-link voltage, $V_{L\text{-}ref}$ is the reference of low-voltage DC bus voltage, u_{dref} is the reference of the output AC voltage, i_{dref} represents feedforward term of the load current. The proposed control structure consists of a central controller and other local controllers. The central controller takes charge of the system-level protection and reference generation. The local controllers of the power module processes tasks such as DC-link voltage control, capacitor voltage balance, low-voltage DC bus voltage control and PWM

signals generation based on the local voltage and current sensors. The local controller of the inverter takes charge of output voltage and current regulations and PWM signals generation. Meanwhile, the load current reference i_{dref} is fed back to the central controller and then it is distributed to each power module in order to improve the dynamic response of the system. The proposed control method regulates the capacitor voltage of the power module based on the local voltage and current sensors. Therefore, there is no need to transmit the voltage information of each power module to the central controller, which greatly reduces the data interaction among the central controller and the local controllers. The reduction of data interaction can reduce the communication burden of the central controller, and also increase the modularity and scalability of the CHB converter-based PET.

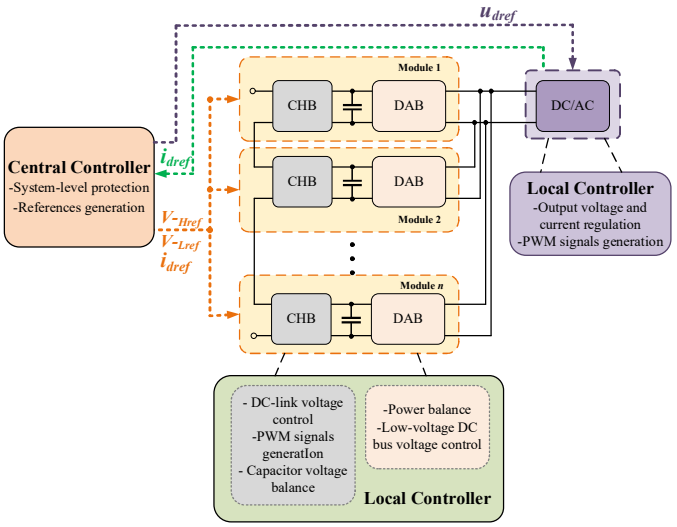

Fig. 2. Proposed distributed feedforward control structure for CHB converter-based PET.

The proposed control method can effectively reduce the calculation and communication burden of the central controller by comparing the communication architectures of the centralized control and the distributed feedforward control. Fig. 3(a) shows the communication architecture of centralized control method, which can be divided into a central controller, an inverter stage local controller, and n local controllers which are used to control n modules, where n represents the number of modules. For the centralized control method, the local controller of each module and the central controller are connected by five optical fibers, and the central controller side contains four output ports and 1 receiving port. Two of the output fiber ports provide PWM signals to the CHB converter, and the other two output fiber ports provide PWM signals to the DAB converter. The receiving fiber port is a high-speed communication port, it receives the sensed voltages and sensed currents as well as the states from local controllers. The central controller sends the PWM signals to the inverter stage local controller via three optical fibers, and receives the sensed voltages and sensed currents as well as the states from the inverter stage by using one high-speed communication receiving port. Fig. 3(b) shows the communication architecture of the proposed distributed feedforward control, which consists of a central controller, an inverter stage local controller and n local controllers which are employed to control CHB converters and DAB converters. From Fig. 3(b), it can be seen that the central controller is connected to the first one local controller through three optical fiber ports. The local controllers are connected to each other with the similar optical fiber ports. Two of them are high-speed communication ports, which are used to exchange the data among the central controller and the local controllers. The other one is a low-speed optical ports, which is employed to transfer the synchronization signal from the central controller to the local controllers. One of the high-speed communication ports sends the command values $V\text{-}_{Href}$, $V\text{-}_{Lref}$ and the feedforward current value i_{dref} to the local controllers. The other one receives the states from the local controllers. The central controller and the inverter stage local controller are also connected through three optical fibers. The central controller sends the output voltage command value u_{dref} to the inverter stage local controller, receives the states and the feedforward current value i_{dref} from the inverter stage local controller.

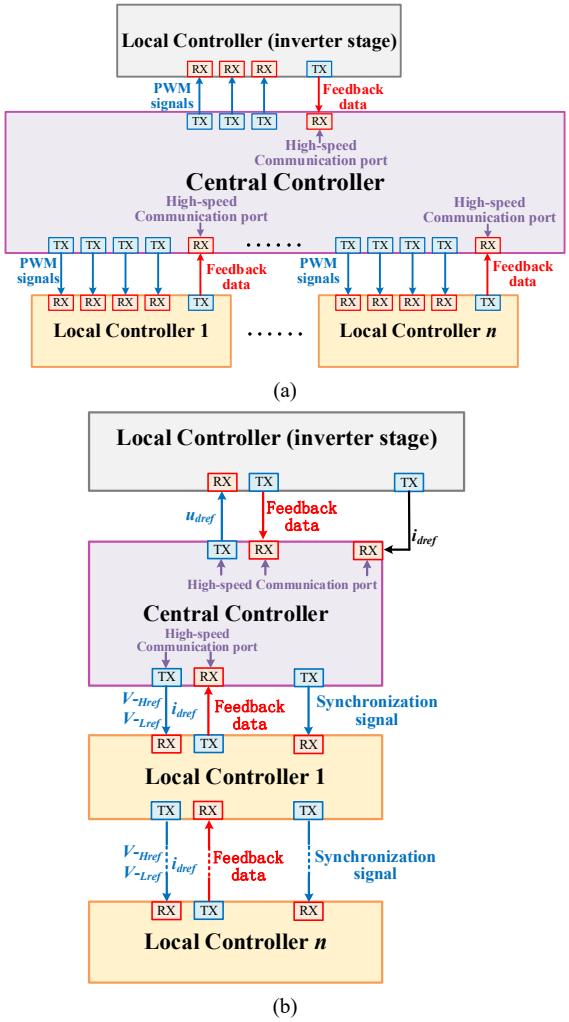

Fig. 3. Different central-local communication architectures. (a) Centralized control communication architecture, (b) Proposed distributed feedforward control communication architecture.

For the centralized control, most of the calculations, such as system-level control, DC-link voltage control, PWM signals generation, capacitor voltage balance, power balance control, low-voltage DC bus voltage control, inverter output voltage

and current regulation, are executed in the central controller, which induces a high computational burden for the central controller. Meanwhile, the sensed voltages and sensed currents as well as the states of each module are fed back to central controller via the high-speed communication links, which induces a high communication burden for the communication network. For the proposed distributed feedforward control, the central controller only processes the tasks of the system-level control, such as system-level protection and references generation, other calculations are distributed to local controllers, so the computational burden for the central controller can be significantly reduced. Meanwhile, the central controller only needs to receive i_{dref} and the states of the local controllers, then send $V\text{-}_{Href}$, $V\text{-}_{Lref}$ and u_{dref} to the local controllers, the communication burden for the communication network is also reduced.

For a PET system with n modules and one inverter stage, the centralized control method needs ($5n$+4) optical fibers to interface the central controller to the local controllers, but the proposed distributed feedforward control method only needs six optical fibers to interface the central controller to the first one local controller and the inverter stage local controller and 3(n-1) optical fibers to interface one local controller to another local controller. Meanwhile, the proposed distributed feedforward control method has good scalability and expandability and it is easy to expand the number of modules.

A. Distributed feedforward control of CHB converters

Fig. 4 shows the rectifier stage topology of the CHB converter-based PET. Define S_i (i=1, 2, …n) as the switching function of module i, T_{ik} is the switching state of power device k in power module i. When T_{ik} is 1, it means that the power device is turned on, and when T_{ik} is 0, it means that the power device is turned off. The switch states of each power module can be expressed as:

$$S_i = T_{i1} \times T_{i4} - T_{i2} \times T_{i3} \tag{1}$$

The switching function S_i has three states. Define the direction of the input current is as shown in Fig. 4. When the switching function S_i is 1, it means that the MV grid charges the capacitor of module i; when the switching function S_i is 0, it means that the module i is bypassed and the MV grid does not charge or discharge the capacitor of module i; when the switching function S_i is -1, it means that the MV grid will discharge the capacitor of module i. Then the following equation can be obtained:

$$L\frac{di_s}{dt} = e_s - R_s i_s - \sum_{i=1}^{n} S_i v_{DCi} \tag{2}$$

where e_s, i_s, and R_s represent input voltage, input current, and MV grid internal resistance, respectively. v_{DCi} is the DC voltage of module i. The average value of the input voltage can be expressed as:

$$v = \sum_{i=1}^{n} S_i v_{DCi} \tag{3}$$

A deadbeat controller is used to regulate the input AC current of each power module. The basic idea of the deadbeat controller is to calculate the pulse width of the next switching cycle based on the system state equations and output feedback signals of the current switching period [15]. For each power module, the time domain circuit equation can be derived:

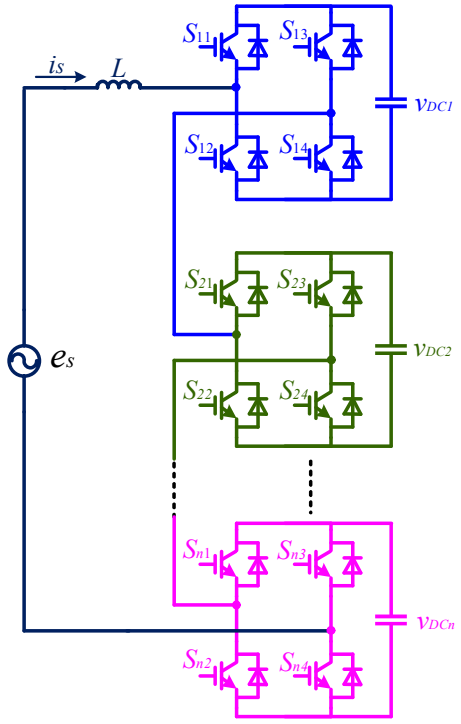

Fig. 4. Rectifier stage of the PET based on CHB.

$$v(t) = -\frac{L}{n}\frac{di(t)}{dt} - \frac{Ri(t)}{n} + \frac{e_s(t)}{n} \tag{4}$$

where $v(t)$ is the average input voltage of the CHB converter at time t, L is the filter inductance, R is the internal resistance of the MV grid, $e_s(t)$ is the MV grid voltage, and n is the number of modules. Then the difference equation within a sampling period can be expressed as:

$$v(k) = -\frac{L}{n \cdot T_s}\left[i(k+1) - i(k)\right] - \frac{Ri(k)}{n} + \frac{e_s(k)}{n} \tag{5}$$

where the sampling period is expressed as T_s. $i(k$+1) and $i(k)$ are the AC current values under the (k+1)th and (k)th sampling period in turn. It is expected that the (k+1)th AC current can track the reference current value, so the reference current value can be replaced by the (k+1)th AC current. Then the following formula can be obtained:

$$v(k) = -\frac{L}{n \cdot T_s}\left[i^*(k+1) - i(k)\right] - \frac{Ri(k)}{n} + \frac{e_s(k)}{n} \tag{6}$$

If v_{DC} represents the DC voltage of each power module of the CHB converter, the duty cycle of the power device in each sampling period can be expressed as:

$$D(k) = \frac{v(k)}{v_{DC}} \tag{7}$$

Incorporating formula (6) into formula (7), the expression of the duty cycle of the power device can be obtained:

$$D(k) = \frac{-\frac{L}{n \cdot T_s}\left[i^*(k+1) - i(k)\right] - \frac{Ri(k)}{n} + \frac{e_s(k)}{n}}{v_{DC}} \tag{8}$$

where $Ri(k)$ is the internal resistance of the MV grid, which can

be ignored under the normal circumstances, so the duty cycle of the power device in each power module is obtained as:

$$D(k)=\frac{-\frac{L}{n\cdot T_s}\left[i^*(k+1)-i(k)\right]+\frac{e_s(k)}{n}}{v_{DC}} \tag{9}$$

In order to keep the output DC voltage of the CHB converter at a fixed reference value, it is necessary to add a voltage outer loop to regulate the average output DC voltage. Since the instantaneous power of the AC input side of each phase has the double grid frequency fluctuations, the capacitor voltage of the CHB will also fluctuate. As a result, only low bandwidth controllers can be used as the voltage outer loop controller. Reference [16] gives a method to eliminate the double grid frequency voltage ripple without a low-pass filter, and the capacitor voltage can be expressed as:

$$V_{DCi}\approx v_{DCi}+B_i=v_{DCi}+\frac{I_g\sqrt{(\omega LI_g)^2+U_g{}^2}}{4\omega C v_{DCi}}\sin(2\omega t+\varphi) \tag{10}$$

$$\varphi=\arctan(\frac{\omega LI_g}{U_g n}) \tag{11}$$

where V_{DCi} is the capacitor voltage of power module i, v_{DCi} is the DC component of the capacitor voltage in the power module i, B_i is the double grid frequency voltage ripple of power module i, I_g is the grid current amplitude, L is the input filter inductance, U_g is the input voltage peak value of each power module, and C is the DC-link capacitance, ω is the angular frequency of the grid, and n is the number of power modules.

In order to further improve the dynamic response of the system, a load current feedforward control is added to the distributed control of the CHB converter, which forms the distributed feedforward control. Since the input and output power of the PET system are equal when the power loss of the system is neglected, the following formula can be obtained:

$$\frac{e_s i_s}{2}=\frac{3u_{dref}i_{dref}}{2} \tag{12}$$

where e_s and i_s are the peak values of the input voltage and current, and u_{dref} and i_{dref} are the peak values of the output reference voltage and current. So the feedforward coefficient k_1, which represents the ratio of the input current to the output current reference, can be expressed as:

$$k_1=\frac{i_s}{i_{dref}}=\frac{3u_{dref}}{e_s} \tag{13}$$

The distributed feedforward control structure of CHB converter is shown in Fig. 5. In Fig. 5, v_{DCi} is the sensed DC-link voltage, $V_{H\text{-}ref}$ is the reference of DC-link voltage, $k_1 i_{dref}$ represents feedforward term of the load current, K_{p1} and K_{i1} are the parameters of the DC-link voltage control, K_{p2} are the parameters of MV gird input current control. The duty ratio of the power device in the next sampling period can be calculated based on the input current, MV grid voltage, input filter inductance and reference current of each power module in the current sampling period, and the current and voltage of the CHB converter can be controlled.

The phase-shifted carrier pulse width modulation (PSC-PWM) is used in the rectifier stage of the CHB converter-based PET. The phase-shift angle among the carriers is 360°/2n as shown in Fig. 6, where n is the number of power modules, V_{i1} (i=1,…,n) represents the carrier waveform of the power device S_{i1} as shown in Fig. 4, V_{i4} represents the carrier waveform of the power device S_{i4}. The modulating waveform u_s is compared with the carrier waveforms, and the driving signals for the power devices are generated. A voltage with 2n+1 levels will be generated on the input MV grid side with n power modules by using PCS-PWM modulation [17]. Meanwhile, it can improve the equivalent switching frequency of the CHB converter.

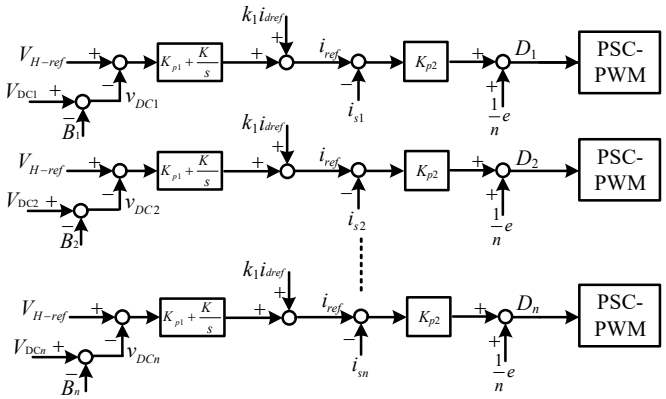

Fig. 5. Distributed feedforward control strategy of CHB converter.

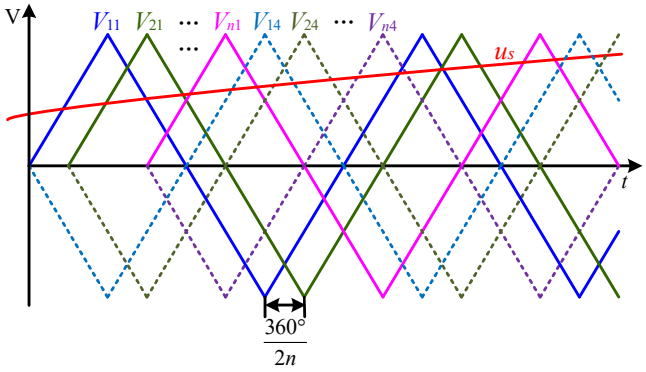

Fig. 6. PSC-PWM principle.

B. Distributed feedforward control of DAB converters

The power of the power modules would be unbalanced without properly control because of the parameter variations of the high frequency transformers and capacitors. The unbalanced power will cause uneven distribution of the voltage or current stress of the switching devices, which will affect the normal operation of the system. Therefore, the power balance control of the module is indispensable and is realized through the isolation stage. A control method based on the phase shift is employed to control the power transfer between the primary side and the secondary side, which is shown in Fig. 7. In Fig. 7, S_{1p}, S_{4p} and S_{1s}, S_{4s} are the switching signals of the primary and secondary power devices; V_p and V_s are the primary side and secondary side voltages of the high frequency transformer; V_p is the high-frequency transformer primary side current; φ is the phase-shift angle of the primary side and secondary side voltages of the high-frequency transformer. The output power of the isolation stage can be expressed as:

$$P=\frac{NV_{H1}V_L\varphi/\pi(1-\varphi/\pi)}{2f_sL} \tag{14}$$

where N is the primary and secondary turns ratio of the high-frequency transformer, V_{H1} and V_L are the primary side and secondary side voltages of the DAB converter, d is the duty cycle, f_s is the switching frequency, and L is the leakage inductance of the high-frequency transformer. It can be seen from (14) that the transfer power of the primary and secondary sides of the DAB converter is controlled by controlling the phase-shift angle φ.

Fig. 8 shows the distributed feedforward control strategy of the DAB converters. Each DAB converter has independent control loops, which can improve the scalability and reliability of the system and achieve better modularity. The method eliminating the double grid frequency voltage ripple without a low-pass filter is also adopted in the DAB converter control. In Fig. 8, v_{DCi} is the sensed input capacitor voltage of the DAB converter, V_L is the sensed low-voltage DC bus voltage, $V_{H\text{-}ref}$ is the reference of the input capacitor voltage, $V_{L\text{-}ref}$ is the reference of low-voltage DC bus voltage, φ_i is the phase-shift angle, $k_2 i_{dref}$ represents feedforward term of the load current, K_{p1} and K_{i1} are the parameters of the capacitor voltage balance control, K_{p2} is the parameters of the low-voltage DC bus voltage balance control.

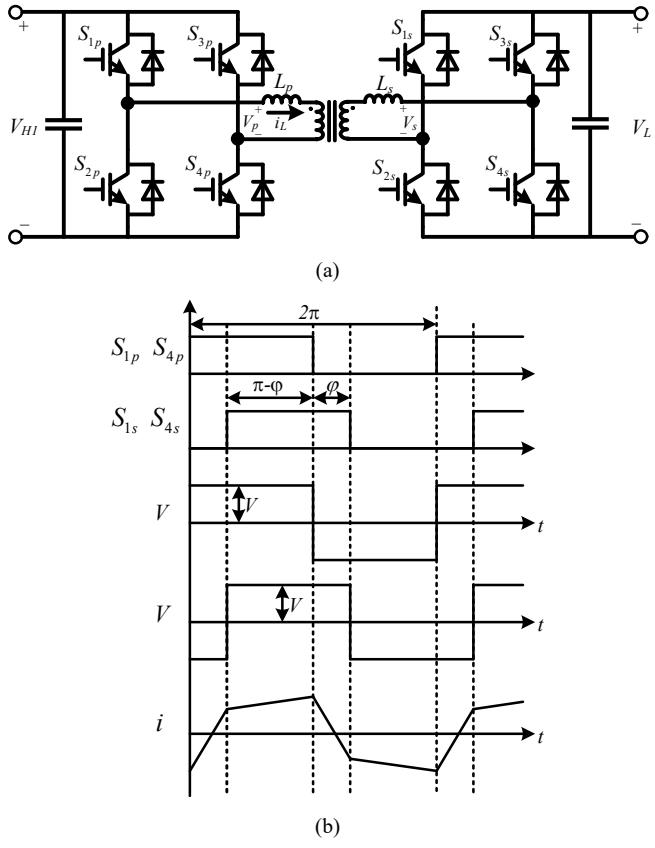

Fig. 7. Phase shift control of DAB converter. (a) DAB converter topology, (b) Phase shift control of DAB converter.

For the *i-th* DAB converter, the sensed input capacitor voltage v_{DCi} is compared with the reference $V_{H\text{-}ref}$, and the error is transferred to the PI regulator to obtain the phase-shift angle compensation value $\Delta\varphi_i$, which contributes the capacitor voltage balance control. Meanwhile, the sensed low-voltage DC bus voltage V_L is compared with the reference $V_{L\text{-}ref}$, and the error is transferred to the PI regulator to obtain a phase-shift angle φ_i', which contributes the low-voltage DC bus voltage control. These two phase-shift angle components and the feedforward term are combined to generate the final phase-shift angle of the DAB converter.

The feedforward term is introduced in order to improve the dynamic response of the system. Since the output power of DAB converters and output power of the PET system are equal when the power loss of the system is neglected, the following formula can be obtained:

$$\frac{nNV_{H1}V_L\varphi/\pi(1-\varphi/\pi)}{2f_sL}=\frac{3}{2}u_{dref}i_{dref} \tag{15}$$

The φ/π（1-φ/π）can be approximately equal to φ/π when φ/π is smaller than 0.3. So the feedforward coefficient k_2, which represents the ratio of the DAB converter phase-shift angle to the output current reference, can be expressed as:

$$k_2=\frac{\varphi}{i_{dref}}=\frac{NV_{H1}V_Ln}{\pi f_sL} \tag{16}$$

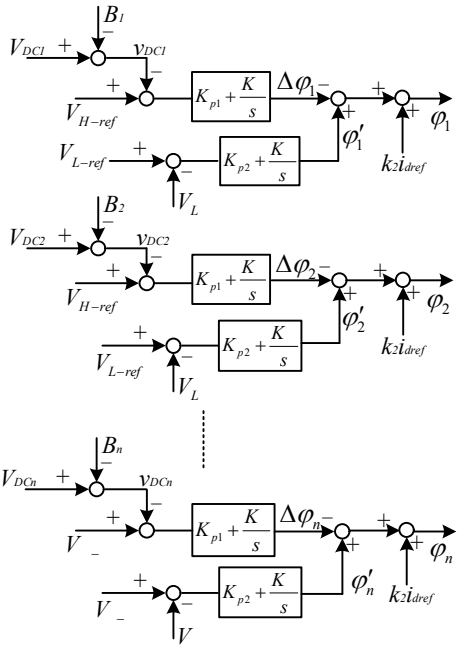

Fig. 8. Distributed feedforward control strategy of DAB converter.

C. Voltage and current regulation of inverter

The inverter stage is realized by a three-phase inverter. The inverter stage is used to regulate the output voltages and currents. The inverter is controlled by a local controller, which is shown in Fig. 2. In the inverter stage, a current inner loop and a voltage outer loop are used to regulate the output voltage and currents. The *d-q* decoupling control method is adopted in the current inner loop and voltage outer loop, as shown in Fig. 9. In Fig. 9, u_{dref}, u_{qref} and i_{dref}, i_{qref} are the *d*-axis and *q*-axis references of the output voltages and currents, u_d, u_q and i_d, i_q are the calculated *d*-axis and *q*-axis values of the sensed output voltages and currents, ω is the angular frequency of the output voltage, C and L are the output capacitance and inductance, u_{d0*}

and u_{q0*} are the outputs of the current regulator.

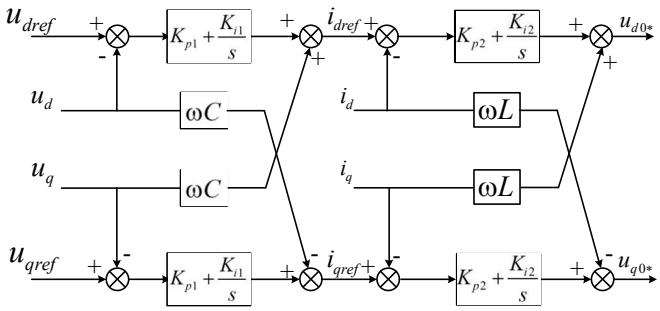

Fig. 9. Voltage and current control of inverter.

The sensed voltages and currents in the stationary coordinate system are converted to the rotating coordinate system. The corresponding park transformations are express as:

$$\begin{pmatrix} u_d \\ u_q \end{pmatrix} = \frac{2}{3}\begin{pmatrix} \cos\theta & \cos(\theta-120°) & \cos(\theta+120°) \\ \sin\theta & \sin(\theta-120°) & \sin(\theta+120°) \end{pmatrix}\begin{pmatrix} v_a \\ v_b \\ v_c \end{pmatrix} \quad (17)$$

$$\begin{pmatrix} i_d \\ i_q \end{pmatrix} = \frac{2}{3}\begin{pmatrix} \cos\theta & \cos(\theta-120°) & \cos(\theta+120°) \\ \sin\theta & \sin(\theta-120°) & \sin(\theta+120°) \end{pmatrix}\begin{pmatrix} i_a \\ i_b \\ i_c \end{pmatrix} \quad (18)$$

where v_a, u_b, u_c and i_a, i_b, i_c are the output voltages and currents. An inverse-park transformation is employed to obtain the modulation signals of the inverter from the outputs of the current regulator u_{d0*} and u_{q0*}. The modulation signals are transferred to the modulator and the PWM signals for the power devices are generated.

IV. Simulation Results

In order to verify the effectiveness of the proposed control method, a simulation model of CHB converter-based PET is established in the MATLAB/simulink. The simulation parameters of the PET are tabulated in Table I. The number of the power module n for each phase is selected as 11 because 1700V power devices are employed in the simulation. For a 10kV power grid system, 1700V power devices can effectively improve the efficiency and power density of the system as well as improve the reliability of the system [18].

TABLE I
Simulation Parameters of PET

Parameters	Value
Number of power modules per phase	11
DC-link voltage	936V
DC-link capacitor	3.7mF
CHB input filter inductor	4mH
Switching frequency of CHB	10kHz
Low-voltage DC bus voltage	936V
Transformer frequency	10kHz
Transformer ratio	1:1
Transformer moves towards inductance	0.23mH
Transformer leakage inductance	5μH/5μH
Transformer capacity	15kVA
Low-voltage DC bus capacitor	15mF
Switching frequency of DAB	10kHz
Inverter output capacitor	47μF
Inverter output inductor	0.8mH
Switching frequency of inverter	5kHz

A. Start-up process of the PET

The start-up process of the PET is shown in Fig. 10, Fig. 11 and Fig. 12. Fig. 10 shows the waveforms of CHB converters when starting the PET. At the beginning of the start-up (t<0 in Fig. 10), all power devices are turned off, the CHB converter is in uncontrolled rectifier mode and the DC-link voltage is 742V as shown in Fig. 11. At t=0, the CHB converters is started and the DC-link voltage are smoothly charged to 936V. At t=0.1s, the primary side of the DAB is started, the duty cycle of the primary side is linearly changed from 0 to 50% while the power devices of the secondary side are still turned off, the voltage of the low-voltage DC bus is smoothly charged. At t=0.21s, the voltage of the low-voltage DC bus is charged to near the steady-state value 936V. At this time, the gate signals of the secondary side power devices are unlocked and the DAB stage is fully started. At t=0.4s, the inverter stage is started and outputs power to the load as shown in Fig.12. The start-up process of the PET system is completed.

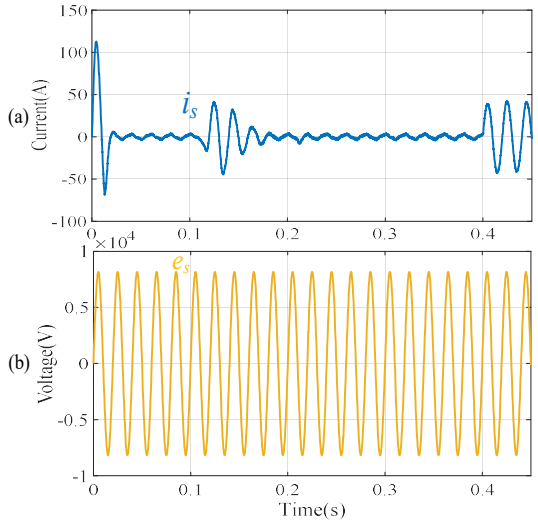

Fig. 10. Waveforms of CHB converters when starting the PET. (a) Input AC current i_s, (b) MV grid voltage e_s.

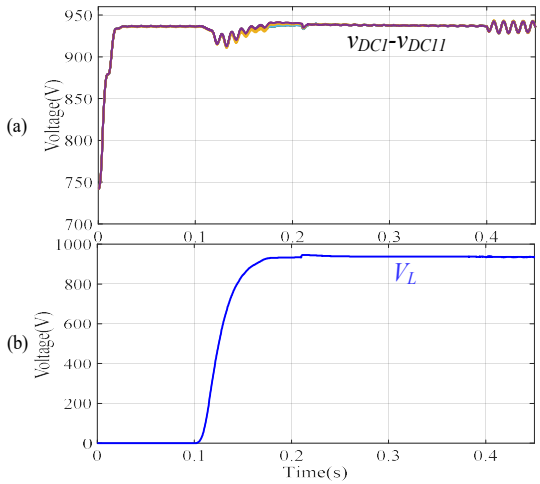

Fig. 11. Waveforms of DC-link voltages and DAB converters when starting the PET. (a) DC-link voltages v_{DC1}~v_{DC11}. (b) Low-voltage DC bus voltage V_L.

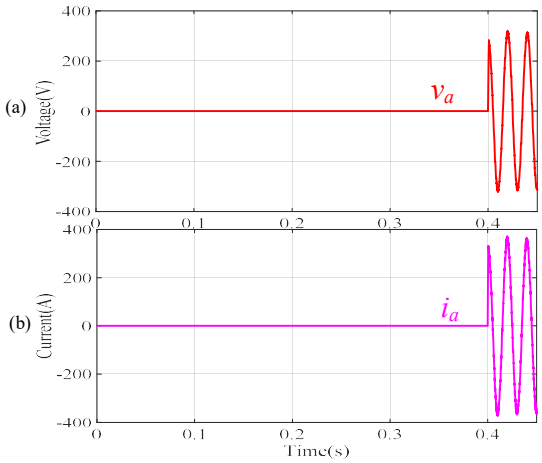

Fig. 12. Inverter stage waveforms when starting the PET. (a) Output AC voltage v_a , (b) Output AC current i_a.

B. Steady-state operation

Fig. 13 shows waveform of CHB converters based the PET, and the MV grid voltage waveform is shown in Fig. 13(a). The DC-link voltage of the each CHB converter is 936V and the number of power modules for each phase is 11, so the modulation ratio is 0.8, which generates a 19-level voltage waveform, as shown in Fig. 13(b). The application of CHB converter can increase the equivalent switching frequency of the rectifier stage. Meanwhile, the harmonics injecting to the MV gird can be effectively reduced. The input AC current waveform of the rectifier stage is shown in Fig. 13(c), which is a pure sinusoidal waveform.

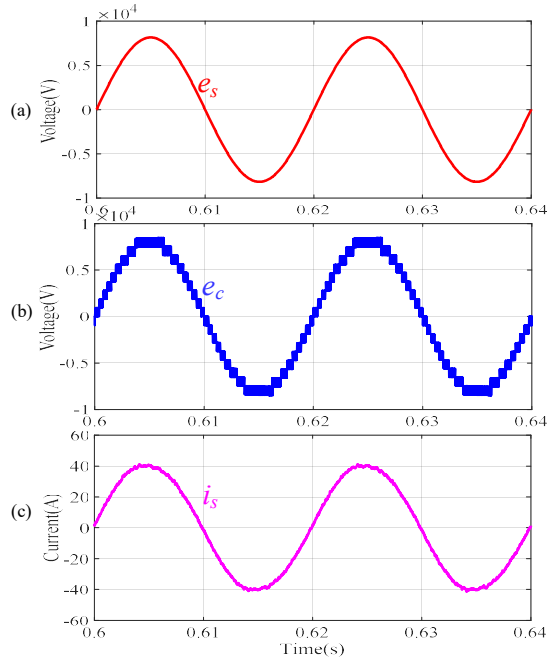

Fig. 13. Waveform of CHB converters. (a) MV grid voltage e_s, (b) Multilevel voltage e_c, (c) Input AC current i_s.

The waveform of the DAB converter is shown in Fig. 14. Fig. 14(a) shows the DC-link voltage waveform of the PET. It can be seen from the simulation results that the DC-link voltages of the eleven power modules are the same, and the voltage of each power module fluctuates around 936V with a small fluctuation range. It is proved that the proposed distributed feedforward control can achieve a good voltage balance for the input capacitor voltages of the DAB converter. The output of these eleven power modules are connected in parallel to form the low-voltage DC bus. The low-voltage DC bus voltage is stable at 936V, as shown in Fig. 14(b), which shows the proposed distributed feedforward control can achieve a good voltage regulation for the low-voltage DC bus voltage.

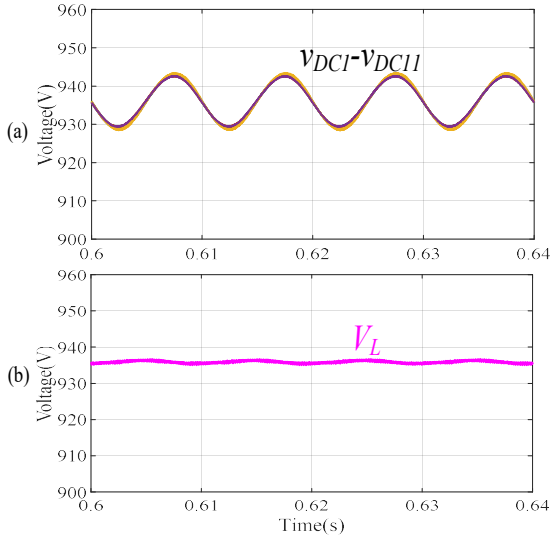

Fig. 14. Waveform of DAB converters. (a) DC-link voltages v_{DC1}~v_{DC11}. (b) Low-voltage DC bus voltage V_L.

The three-phase output voltage and current waveforms of the inverter are shown in Fig. 15(a) and Fig. 15(b), respectively. The rated AC output phase voltage is 220V, which is a pure sinusoidal waveform as shown in Fig. 15(a). The peak value of the output current is 365.3A, which is a good sinusoidal waveform with small current ripples as shown in Fig. 15(b).

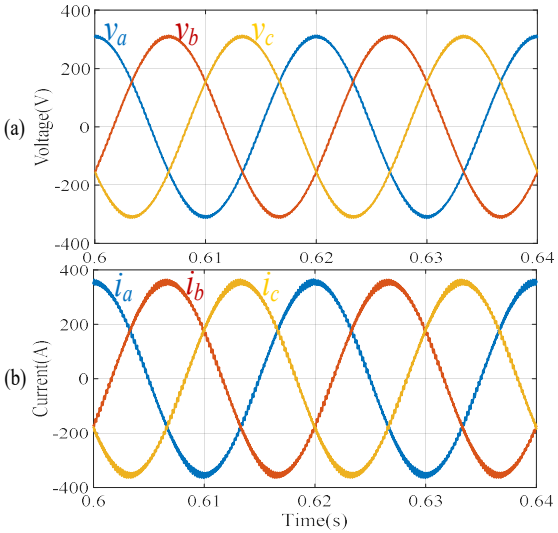

Fig. 15. Inverter waveform. (a) Three-phase Output voltage v_a v_b v_c , (b) Three-phase Output current i_a i_b i_c .

C. Dynamic response

In order to evaluate the dynamic response of the proposed distributed feedforward control method, a load current step changing is simulated. At the time of t=0.8s, the resistance of the load resistor is doubled. Fig. 16 shows the dynamic

response of the waveform on the high voltage side. Fig. 16(a) shows the MV grid input current of the CHB converter during the load resistor step changing. The input AC current can achieve its steady-state quickly after the load resistor step changing. Fig. 16(b) shows the DC-link voltage waveform of the CHB converter with or without the proposed distributed feedforward control method. The simulation results clearly show significantly improvement of the dynamic response by using the proposed control method.

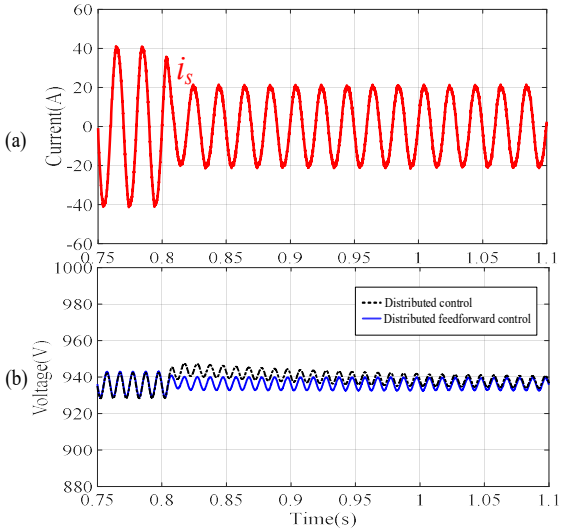

Fig. 16. High-voltage side waveform when the load resistor step changing. (a) High-voltage side input current i_s, (b) DC-link voltage with or without proposed distributed feedforward control method.

Fig. 17 shows the dynamic response of the waveform on the low voltage side. Fig. 17(a) shows the low-voltage DC bus voltage waveform with or without the proposed distributed feedforward control method. The simulation results also clearly show significantly improvement of the dynamic response by using the proposed control method. In order to observe the dynamic response of the output current more clearly and intuitively, Fig. 17(b) shows the *a* phase output AC current waveform of the inverter, omitting the other two phases. The output AC current can achieve its steady-state quickly after the load resistor step changing.

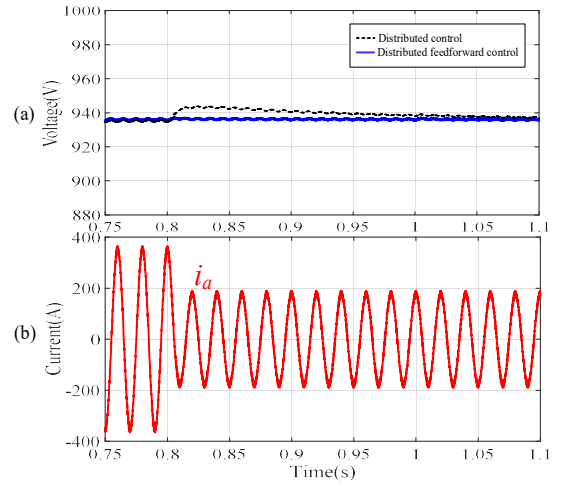

Fig. 17. Low-voltage side waveform when the load resistor step changing. (a) Low-voltage DC bus voltage with or without proposed distributed feedforward control method. (b) Phase *a* output AC current i_a.

V. CONCLUSIONS

This paper proposes a distributed feedforward control method for the CHB converter-based PET to overcome the disadvantages of existing centralized control method. The proposed distributed control method assigns most of the computation to the local controller, so the computational and communication burden of the central controller is significantly reduced. Through distributed feedforward control, each power module performs the independent control loops by their own, which makes the system control more modularization and improves the reliability and scalability of the system. Meanwhile, a load current feedforward control is introduced to DC-link voltage control and the DAB converter control, which significantly improve the dynamic response of the system. Finally, a simulation model is built and the effectiveness of the proposed control method is verified.

REFERENCES

[1] Li Zixin, Gao Fanqiang, Zhao Cong, et al. "Research Review of Power Electronic Transformer Technologies," *Proceedings of the CSEE*, vol. 38, no. 5, pp. 1274-1289, 2018.

[2] Li Zixin; Wang Ping; Chu Zunfang, et al. "Research on Medium-and High-Voltage Smart Distribution Grid Oriented Power Electronic Transformer," *Power System Technology*, no. 9, pp. 2592-2601, 2013.

[3] She, Xu; Huang, AlexQ; Burgos, Rolando. "Review of Solid-State Transformer Technologies and Their Application in Power Distribution Systems," *IEEE JOURNAL OF EMERGING AND SELECTED TOPICS IN POWER ELECTRONICS*, Vol.1,no. 3, pp. 186-198, 2013.

[4] Huang, A.Q.; Crow, M.L.; Heydt, G.T.; Zheng, J.P.; Dale, S.J.. "The future renewable electric energy delivery and management (FREEDM) system: The energy internet (Article)," *Proceedings of the IEEE*, vol. 99, no. 1, pp. 133-148, 2011.

[5] Li Gong, Ke Dai, Jingjing Chen, et al. "Design and implementation of distributed control system for cascaded H-Bridge multilevel STATCOM," in *Proc. of Conference Proceedings - IEEE Applied Power Electronics Conference and Exposition APEC*., Fort Worth, TX. 2011.

[6] Wenxi Yao ; Jian Liu ; Zhengyu Lu , "Distributed Control for the Modular Multilevel Matrix Converter..," *IEEE Transactions on Power Electronics*, vol. 34, no. 4, pp. 3775-3788, 2019.

[7] E. Villanueva, P. Correa, J. Rodr´ıguez, and M. Pacas, "Control of a single-phase cascaded h-bridge multilevel inverter for grid-connected photovoltaic systems," *IEEE Transactions on Industrial Electronics*, vol. 56, no. 11, pp. 4399–4406, 2009.

[8] H. Zhao, T. Jin, S. Wang, and L. Sun, "A real-time selective harmonic elimination based on a transient-free inner closed-loop control for cascaded multilevel inverters," *IEEE Transactions on Power Electronics*, vol. 31, no. 2, pp. 1000–1014, 2016.

[9] Xu, B.; Tu, H.; Du, Y.; Yu, H.; Liang, H.; Lukic, S. "A distributed control architecture for cascaded H-bridge converter," in *Proc. of Conference Proceedings-IEEE Applied Power Electronics Conference and Exposition - APEC*, pp. 3032-3038, 2019.

[10] Nie J, Yuan L, Gu Q, et al. "A Coordinate and Distributed Control Scheme for Multilevel and Multi-Stage Medium Voltage Solid State Transformer" *IPEC-Niigata*, ECCE Asia. 2018.

[11] Hou, Xiaochao; Sun, Yao; Han, Hua; Liu, Zhangjie; Su, Mei; Wang, Benfei; Zhang, Xin, " A General Decentralized Control Scheme for Medium-/High-Voltage Cascaded STATCOM.," *IEEE Transactions on Power Systems*, vol. 33, no. 6, pp. 7296-7300, 2018.

[12] McGrath, Brendan P; Holmes, Donald Grahame; Kong, Wang Y " A Decentralized controller architecture for a cascaded H-bridge multilevel converter," IEEE Transactions on Industrial Electronics, vol. 61, no. 3, pp. 1169-1178, 2014.

[13] Cao Yang; Yuan Liqiang; Zhu Shaomin, "Parameter Design of Energy Router Orienting Energy Internet," *Power System Technology*, vol. 39, no. 11, pp. 3094-3101, 2015.

[14] Wang Shanshan; Wang Yubin; Lin Yifei; Yu Chenghao; Li Houzh, " Voltage and Power Balance Control for Cascaded Multilevel Converter Based Power Electronic Transformer," *Transactions of China Electrotechnical Society*, vol. 31, no. 22, pp. 92-99, 2016.

[15] Shi Wenting, " Improved deadbeat power predictive control of PWM rectifier without grid voltage sensor," M.S. Xi'an University of Technology, Xi'an, China 2019.

[16] Fanbo He; Zhengming Zhao;Liqiang Yuan; Sizhao Lu. "A DC-link voltage control scheme for single-phase grid-connected PV inverters" Energy Conversion Congress and Exposition (ECCE). Phoenix, AZ, 2011.

[17] Holmes, Donald Grahame; McGrath, Brendan P.." Opportunities for harmonic cancellation with carrier-based PWM for two-level and multilevel cascaded inverters," *IEEE Transactions on Industry Applications*, Vol.37,no. 2, pp. 574-582, 2001.

[18] Huber, J.E. 1 ; Kolar, J.W. 1 , " Optimum Number of Cascaded Cells for High-Power Medium-Voltage AC-DC Converters," *IEEE Journal of Emerging and Selected Topics in Power Electronics*, vol. 5, no. 1, pp. 213-232, 2017.

Sizhao Lu (M'16) received the B.S. and M.S. degree in electrical engineering from Harbin Institute of Technology, Harbin, China, in 2008 and 2010, respectively. He received the Ph.D. degree in electrical engineering from Tsinghua University, Beijing, China, in 2016. He joined the Faculty of Electric Power Engineering, Kunming University of Science and Technology (KUST), Kunming, China, in 2016, where he is currently an associate professor with the Department of Electrical Engineering. He was a Visiting Scholar at the Center for Power Electronics Systems, Virginia Tech, Blacksburg, VA, USA, from February 2012 to November 2013.

His research interests include Power Electronic Transformer(PET), Modular Multilevel Converters (MMC), high-frequency high-power DC-DC converters and wireless power transfer (WPT) systems.

Di Zhao received the B.S. degree in electrical engineering from Kunming University of Science and Technology, Kunming, China, in 2018. She is currently working toward the M.S. degree with the Department of Electrical Engineering, Kunming University of Science and Technology, Kunming, China. Her research interests include Power Electronic Transformer(PET) and high-frequency high-power DC-DC converters.

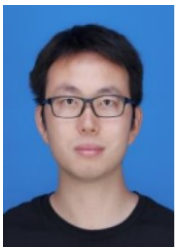

Kai Li (S'13-M'18) received the B.S. degree in electrical engineering from Wuhan University, Wuhan, Hubei, China, in 2011, and the Ph.D. degree from Tsinghua University, Beijing, China, in 2017.

He was a Visiting Scholar with the Center for Power Electronics Systems, Virginia Tech, Blacksburg, VA, USA, from 2013 to 2015. He was a Post-Doctoral Fellow with Tsinghua University from 2017 to 2019. In 2019, he joined the School of Electrical Engineering, Beijing Jiaotong University, Beijing, China, as a lecturer.

His current research interests include solid-state transformer, railway electrification system, modular multilevel converters and so on.

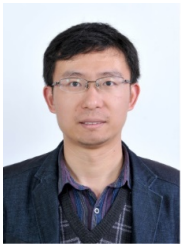

Siqi Li (M'11) received the B.S. and Ph.D. degree in electrical engineering from Tsinghua University, Beijing, China, in 2004 and 2010, respectively. He was a Postdoctoral Fellow with the University of Michigan, Dearborn, USA from 2011 to 2013. In 2013, he joined the Faculty of Electric Power Engineering, Kunming University of Science and Technology (KUST), Kunming, China, where he is currently a professor with the Department of Electrical Engineering. Also, he is the director of the Advanced Power Electronics and New Energy Laboratory in KUST. He was a visiting scholar in San Diego State University from 2018 to 2019.

His research interest focuses on battery management system, high performance wired, wireless battery chargers for electric vehicles and solid state transformers.